Numerical simulation of dissimilar metal welding and its verification for determination of residual stresses

Sz. Szávai http://orcid.org/0000-0002-8311-2870
Bay Zoltán Nonprofit Ltd., Engineering Division
szabolcs.szavai@bayzoltan.hu

Z. Bezi
Bay Zoltán Nonprofit Ltd., Engineering Division
zoltan.bezi@bayzoltan.hu

C. Ohms
European Commission Joint Research Centre, Institute for Energy and Transport
carsten.ohms@ec.europa.eu

ABSTRACT. This paper summarizes the results of the through-thickness residual stress distributions on dissimilar metal weld (DMW) mock-up. DMWs, as welded joints between ferritic steels and either austenitic stainless steels or nickel-based alloys, are commonly found in piping systems of NPPs as well as in other industrial plants. The welding of the mock-up is simulated by the 3D finite element model using temperature and phase dependent material properties. The commercial finite element code MSC.Marc is used to obtain the numerical results by implementing the Goldak's double ellipsoidal shaped weld heat source and combined convection radiation boundary conditions. Residual stress measurements are performed on welded joints to validate the simulation results. The validated residual stress distributions can be used for the life time assessment and failure mode predictions of the welded joints.

KEYWORDS. Dissimilar metal welding; Finite element analysis; Residual stress; Phase transformation.

INTRODUCTION

Dissimilar metal welds are generally used in piping systems of nuclear power plants as well as in other industrial plants to connect low alloy ferritic steel components and austenitic stainless steel or nickel-based alloys. DMWs are produced by fusion welding and their structural stability is strongly affected by welding conditions and post weld heat treatment.

This type of welding process produces large residual stresses. The maximum value of tensile stress is commonly equal to the yield strength of joint materials. The residual stress of welding can significantly impair the performance and reliability of welded structures. The integrity assessment and life estimation for such welded structures require consideration of residual stresses. Therefore, it is necessary to map and assess the distribution of these residual stresses in welded joints.

The mock-up reflects the DMW configuration of the WWER-440 reactors connecting the reactor pressure vessel with the hot-cold leg. It involves a bimetallic fusion weld with three buttering layers towards the ferritic side.
The goal of the mock-up is to replicate the conditions of a heterogeneous weld in a type of WWER 400 RPV nozzle.
In this paper, a 3D thermal-mechanical-metallurgical finite element (FE) model has been developed to investigate the distribution of residual stress. The results of FE analyses were compared with the experimental measurements in the ferritic steel section of the mock-up. The measurement of residual stresses was performed using neutron diffraction. The experimental procedures including sample fabrication and residual stress measurements were followed by the modelling results.

EXPERIMENTAL PROCEDURE

The experimental mock-up as shown in Fig. 1 was manufactured for measuring the final residual stresses. Originally, steel 15H2MFA (Tab. 1) was the manufacture material for the nozzle rings of DN 500 nozzles. This steel has a high stability of mechanical properties including the resistance against temper brittleness and temperature ageing. The safe-ends of DN 500 nozzles were manufactured from austenitic steel 08H18N10T. However this type of steel is no longer available so it is substituted with X6CrNiTi18-10 (1.4541), which has a similar chemical composition, as it can be seen in Tab. 2 The base materials are widely different (15H2MFA ferritic steel and X6CrNiTi18-10 austenitic steel) so in order to perform the welding a transient cladding or cushion has to be implemented.

Figure 1: The mock-up.

C	Si	Mn	S	P	Cr	Ni	Mo	V	Cu
0.13	0.17	0.3	0.025	0.025	2.5	0.4	0.6	0.25	0.15

Table 1: Chemical composition of 15H2MFA steel (wt%).

This cushion has two layers. The thickness of the first layer is 3 ± 1 mm and it was welded on by EA-395/9, Ø 4 mm covered stick electrodes. After the first layer was grinded down to meet the thickness criteria, the second layer was welded on, using EA-400/10T Ø 4 mm covered stick electrodes (the maximal temperature at the time of welding was 100°C on the same conditions as at the 1st layer). The total thickness of the layers has to be 9±1 mm (Fig. 3). The welding parameters are detailed in

Table 3. After cladding, the specimen was heat treated by heating it up to 670°C at a rate of 50°C/h for 16 hours and let it cool down together with the furnace.

	C	Si	Mn	Cr	Ni	Mo	Co	Ti
EA-395/9	0.08	0.35	1.2	13.5	23	4.5	0.08	-
EA-400/10T	0.07	0.5	1.5	17	9.5	2	-	-
316L	0.015	0.4	1.75	18.5	12	2.75	-	-
X6CrNiTi18-10	0.08	0.08	1.5	17	9	-	-	0.4

Table 2: Chemical composition of stainless steels (wt %).

	Welding Process	Current (A)	Voltage (V)	Type of Current and Polarity	Heat Input (kJ/mm)
1st layer	SMAW	120-130	24-25	DCEP	~0.61
2nd layer	SMAW	130-140	25-26	DCEP	~0.69

Table 3: Welding parameters of the cladding.

The welding was performed in two steps and without pre-heating or heat treatment. Originally the root weld was welded manually from the root side by GTAW method using Sv-04H19N11M3 Ø 1.6 mm electrodes in flat position.

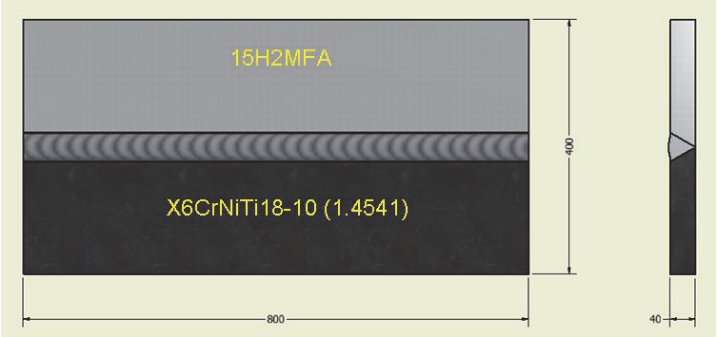

Figure 2: Dimensions of the specimen.

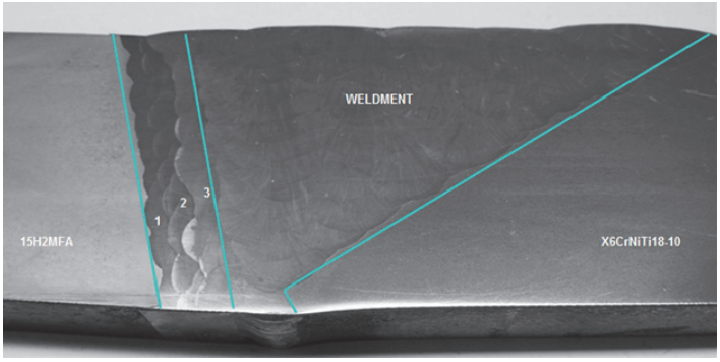

Figure 3: Macrostructures of butt-welded joint.

Unfortunately, this type of electrode is no longer commercially available so a slightly different type of electrode is used, namely Lincoln TIG 316L. As it can be seen from Tab. 2, its chemical composition is almost the same as the Sv-04H19N11M3. The filling weld and the capping were welded by SAW method using Sv-04H19N11M3 Ø 2 mm electrodes and OF-6 flux in horizontal position (Fig. 3).
However, this type of electrode and flux is also outdated and therefore no longer available. The substitution was LNS 316L with P240 flux. The chemical composition of the original and the substitute material has an almost perfect match and the P240 is also a highly basic fluoride agglomerated flux, with a basicity of three, just like the original OF-6 according to [1] and [2]. The welding parameters are detailed in Tab. 4.

	Welding Process	Current (A)	Voltage (V)	Type of Current and Polarity	Heat Input (kJ/mm)
Root weld	GTAW	50-60	12-13	DCEN	~0.1
Filling weld	SAW	320-330	28-29	DCEP	~1.16

Table 4: Welding parameters.

3-D FINITE ELEMENT MODELLING

The welding of DMW mock-up is simulated using three-dimensional (3D) thermo-mechanical and metallurgical finite element model. Work tasks:

- Simulate the cladding process
- Simulate the heat treatment after the cladding
- Simulate the butt-weld process

The FEM pre-processing, calculations and post-processing have been carried out by MSC.Marc and Simufact.welding software based on MSC.Marc code. The thermo-elastic-plastic-metallurgic finite element computational procedure is performed to analyse the welding temperature field and the welding residual stress in DMW mock-up (Fig. 2).
The thermo-mechanical and metallurgical behaviour is calculated using a coupled formulation.

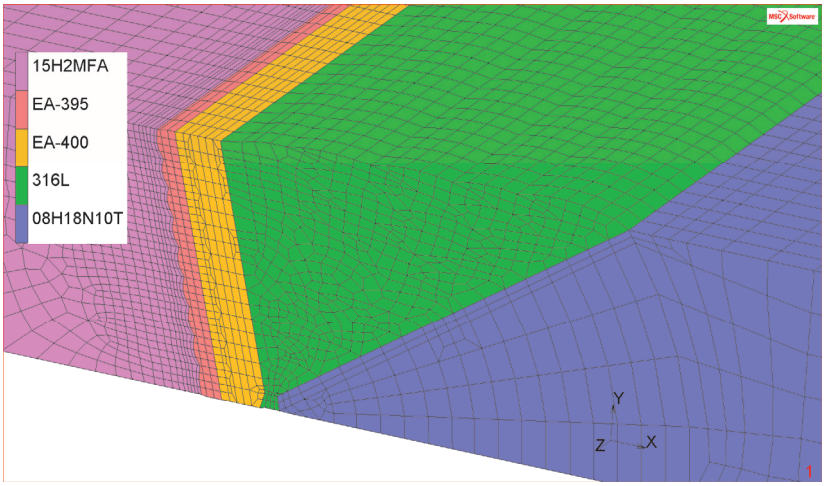

Figure 4: FE mesh for DMW.

The simulations (in 3D) are done on simplified geometries (Fig. 4). In case of cladding, the welded plate was 200 mm instead of 780 mm, due to the high costs of computing time and computer resources compare to the case of welding simulation for the full length plate.
One cladding layer is divided to 9 beads along the plate thickness (40 mm). The number of cladding layers was four. In case of welding process, 200 mm length of weld plate is taken account and the total numbers of simulated passes are 39

(Fig. 5). Between welding of the layers ~5 min cooling time is considered, because the interpass cooling temperature is important factor in the final residual stress distribution. Interpass temperature was 250°C in the first cladding layer and it was under 100°C in the other cladding layers and all layer of butt-weld.

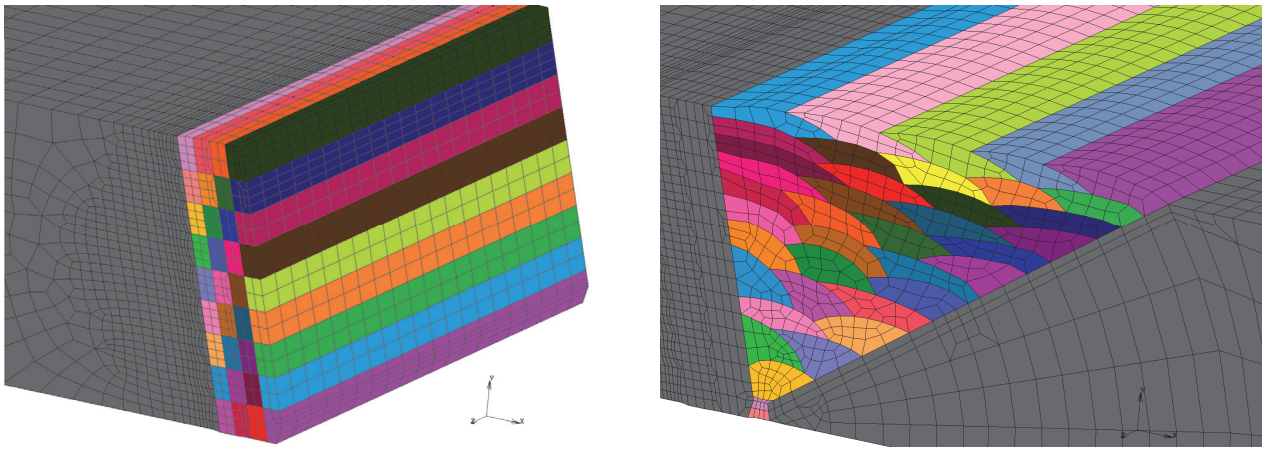

a) Cladding passes b) Weld passes

Figure 5: Welding layers.

For DMW simulation, the FE models are created by 8-noded hexagonal elements, number of element is 64120, and number of nodes is 68798. The 15H2MFA plate is modelled as simply supported, during both the cladding sequences and butt-weld sequences.
Due to the expected high temperature and stress gradients near the heat source, a relatively fine mesh is used. Element sizes increase progressively with distance from the heat affected zone. In case of butt-weld a relatively coarser mesh is used.
MSC.Marc software uses Goldak's heat source model for welding simulation. The heat source distribution combines two different ellipses, i.e. one in the front quadrant of the heat source and the other in the rear quadrant. Goldak's double ellipsoidal shaped weld heat source can be used to specify volume fluxes in 3D as it is presented in [3] and [5].
MSC.MARC code contains the implementation of material addition or removal technique is very suitable for simulating welding processes [4]. The technique requires that the complete model, including all material volume during the whole process, to be defined and meshed in advance. In the deactivated element method, filler elements are initially deactivated in the analysis and are not shown on the post file. When the elements are physically created by the moving heat source, they are activated in the model and appear on the post file.
Inactive elements have been activated initially to simulate the addition of filler material. The thermal and mechanical activation of the elements are separated. The criterion for thermal activation is that an element should be inside the volume of the heat source. Mechanical activation of an element is achieved when the temperature in the element has dropped below a threshold value. The chosen threshold value is 1800 K.
On all free surfaces of all FE-models a convective heat loss with a heat transfer coefficient, h=15W/mK and a radiation heat loss using an emissivity coefficient, ε=0.5 are defined.
Full Newton–Raphson iterative solution technique with direct sparse matrix solver is used for obtaining a solution. During the thermal analysis, the temperature and the temperature-dependent material properties change very rapidly [5]. Thus, it is believed that a full Newton–Raphson technique using modified material properties gives more accurate results.

MATERIAL PROPERTIES

In order to capture the correct microstructure evolution a number of material properties are required for present simulations (Fig. 4). The elastic behaviour is modelled using the isotropic Hooke's rule with temperature-dependent Young's modulus. The thermal strain is considered in the model using thermal expansion coefficient. The yield criterion is the Von Mises yield surface. In the model, the strain hardening is taken into account using the isotropic Hooke's law for ferritic steel.

The thermo-metallurgy material properties of 15H2MFA steel were generated with JMatPro software [7] based on its chemical composition (Tab. 1). Strain hardenings of the phases at room temperature are shown in Fig. 6. Transformation data was calculated using Simufact.premap interface with 8 μm grain size starting at 1200°C.

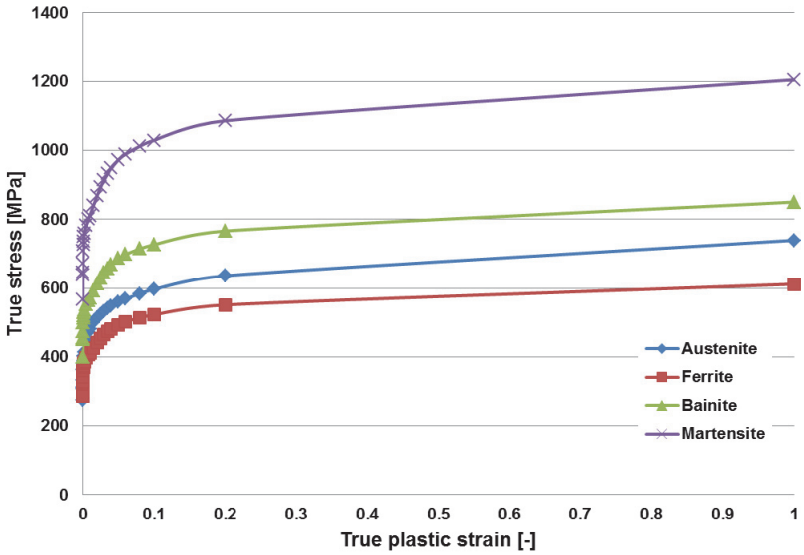

Figure 6: Strain hardening of phases for 15H2MFA.

Stainless steel has no solid-state phase transformation during cooling and the heating time is relatively short, it can be expected that the strains due to phase transformation and creep can be neglected in the present simulation. In case of stainless steels, the strain hardening is taken into account using the Chaboche's combined hardening law [6]. The model in MSC.Marc requires at least five parameters (c, γ, Q, b, σ_y) which is an acceptable number to be determined from experimental stress vs. strain curves (Tab. 5). Using these parameters, the model provides an adequate description of the real elastic-plastic material behaviour.

	σ_y [MPa]	Q [MPa]	b	C [MPa]	γ
EA-395/9	365	1500	50	3000	6
EA-400/10T	420	500	50	1900	3.5
316L	280	600	125	1700	3.2
X6CrNiTi18-10	270	300	50	1800	1.9

Table 5: Mechanical properties at room temperature.

	Modulus of elasticity (Austenite) [GPa]	Modulus of elasticity (F./M.B./P.) [GPa]	Specific heat capacity (Austenite) [kJ/kg°C]	Specific heat capacity (F./M./B./P.) [kJ/kg°C]	Thermal expansion (Austenite) [1/°C*10^{-5}]	Thermal expansion (F./M./B./P.) [1/°C*10^{-5}]	Thermal Conductivity (Austenite) [W/m°C]	Thermal Conductivity (F./M./B./P.) [W/m°C]
EA-395/9	212	-	0.434	-	1.623	-	11.95	-
EA-400/10T	203	-	0.443	-	1.831	-	13.46	-
316L	198	-	0.444	-	1.872	-	13.59	-
X6CrNiTi18-10	196	-	0.450	-	1.898	-	14.12	-
15H2MFA	197	212	0.451	0.446	2.431	1.251	17.28	28.77

Table 6: Thermo-mechanical properties at room temperature.

Other thermo-mechanical material properties of austenitic steels (Tab. 6) were generated by JMatPro software which can be seen from the chemical composition listed in Tab. 2.
The mixture of the initial microstructure elements in the FE model has to be defined for each material. In case of 15H2MFA 100% bainite and for other materials 100% austenite initial fractions were used [2].

MEASUREMENT OF RESIDUAL STRESS

The measurements have been performed at the residual stress diffractometers at beam tubes HB4 and HB5 at the High Flux Reactor (HFR) of the Joint Research Centre in Petten [2].
Measurements in the welding transverse and plate normal directions have been performed in the ferritic steel section on the diffractometer at HB5. For the welding longitudinal direction, the specimen was mounted on the diffractometer at HB4. Fig. 7 shows the section of the Mock-up during these latter measurements on the table of HB4.

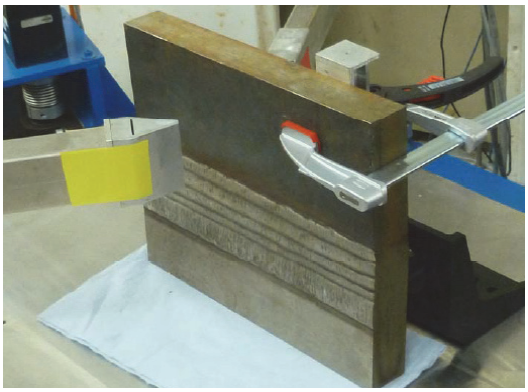

Figure 7: Section of Mock-up on diffractometer.

The measurement positions were located along a number of parallel lines – mostly 6.66 mm apart – oriented in the welding transverse direction ranging from 3 mm to about 45 mm from the interface between the ferritic steel and the buttering layer. The measurement lines were located at mid-length of the Mock-up section in order to minimize the influence of end effects on the results. Because of the thickness of the Mock-up – 40 mm in the ferritic part – it was necessary to work with relatively large sampling volumes, i.e., 7.5 by 6 by 8 mm^3 for the welding longitudinal direction (HB4) and 5 by 4 by 15 mm^3 for the other two directions (HB5) [2].
Stresses were derived from the strains measured in the three directions using the generalized Hooke's law.

RESULTS AND DISCUSSION

DMW model was validated with available experimental results. A simulation model has been developed and extensive numerical calculations were carried out to find out the residual stress distribution of DMW. The deformed mesh contour and photograph of DMW section are compared in Fig. 8. The model distortion and the size of the fusion zone and the heat affected zone (HAZ) are in good agreement with the experimental observations.

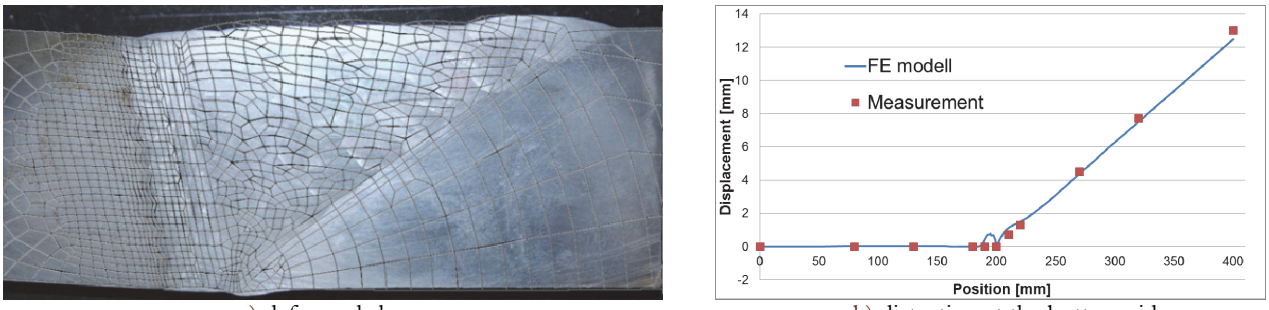

a) deformed shape b) distortion at the bottom side

Figure 8: Distortion after welding.

The results of the simulation provide the size of the HAZ and the volume of the molten zone. The molten zone is the region of the mock-up where the actual weld is formed, while the heat affected zone is the adjacent region where heat may

cause solid state phase transformation, but melting does not occur. An additional capability of the model is the ability to predict the volume fraction of various phases.

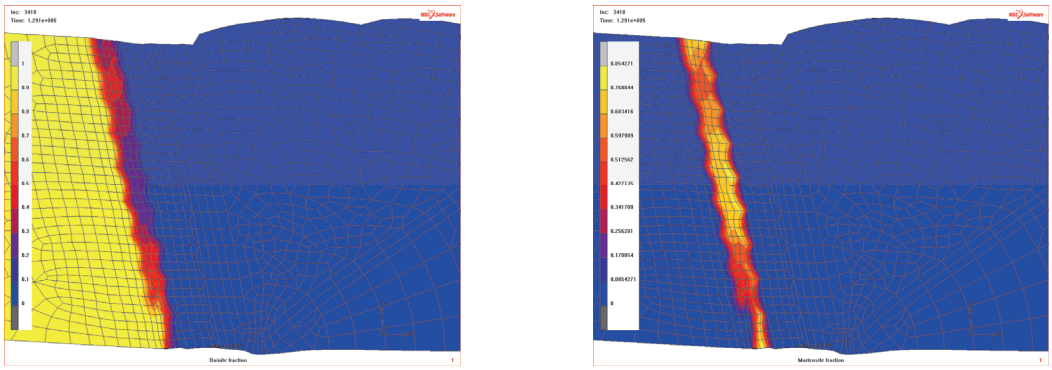

a) bainite fraction b) martensite fraction

Figure 9: Fraction of each phase after welding

The volume fraction of bainite and martensite (Fig. 9) can be quantified and serve as an additional response that can be used to validate this model with experiments and to predict phase volume fractions under new processing conditions. Fig. 10 represents the residual stress distributions of the model after welding. As expected, generally lower stresses in base metal and higher stresses in HAZs as well as welded zones were calculated.

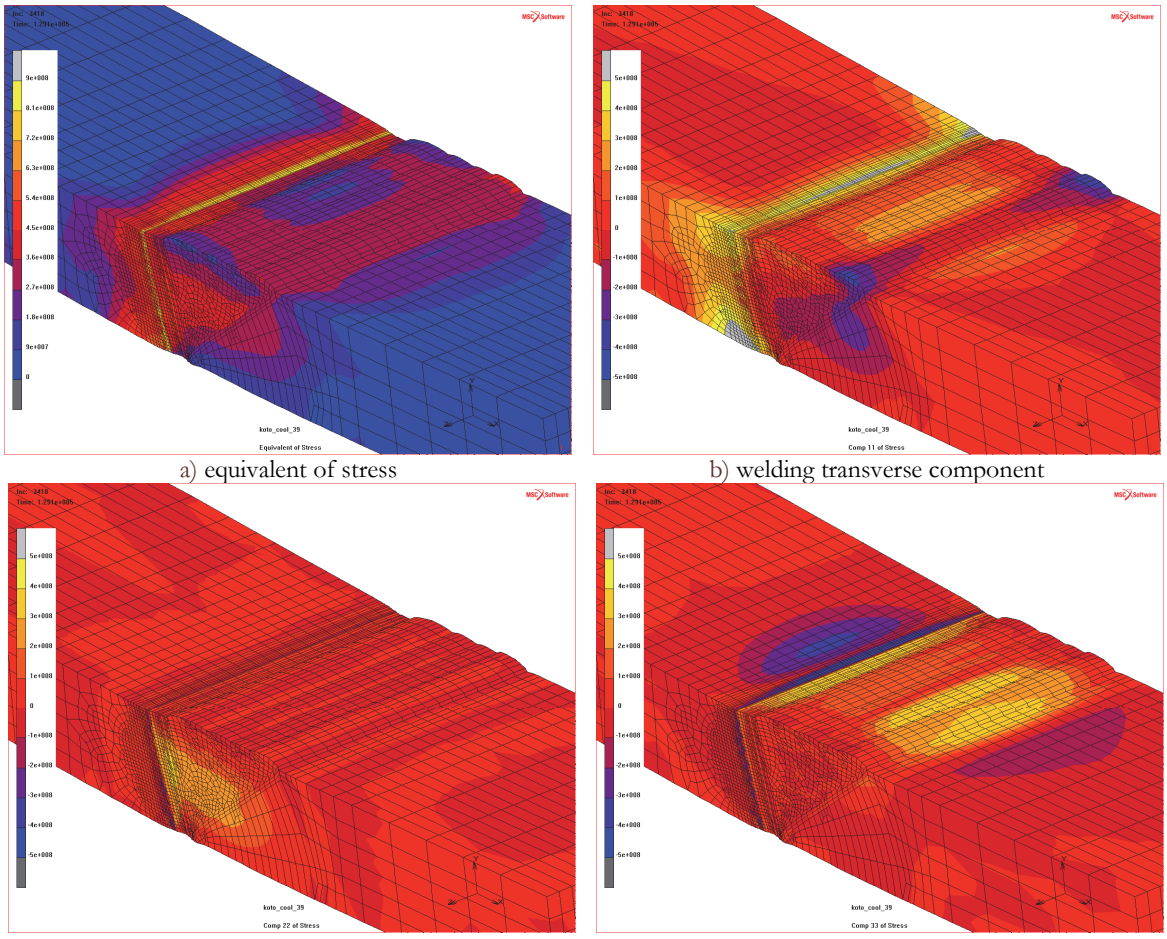

a) equivalent of stress b) welding transverse component

c) through thickness component d) welding longitudinal component

Figure 10: Predicted residual stress distributions [Pa] after but-weld.

From the FE analysis all the stress components are available. Longitudinal, transverse and through thickness are used to denote the residual stress components of three perpendicular directions. The resolution of the measurements is in the order of 6 to 8 mm. The neutron diffraction measurements were not possible closer to the interface than 3 mm. The simulation results and the measured data are compared along three lines on the ferritic section.
Figs. 10-12 show the derived residual stress component for lines at 3.33 mm, 23.33 mm and 33.33 mm from the top surface of the weld plate. In Fig. 10 tensile stresses can be seen near the interface (3.33 mm) for the welding transverse (almost 300 MPa) and the welding longitudinal (about 200 MPa), whereas the through thickness component shows nearly no stress as it should be for this near surface line.

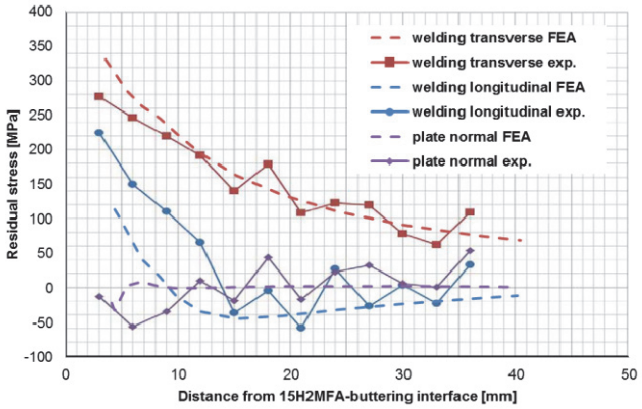

Figure 11: Estimate of residual stresses along a line 3.33 mm from the specimen surface.

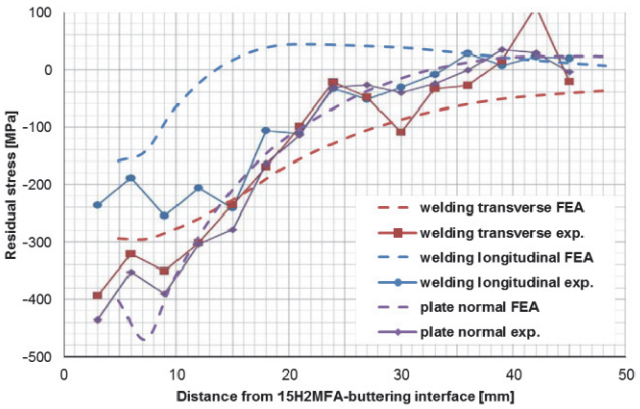

Figure 12: Estimate of residual stresses along a line 23.33 mm from the specimen surface.

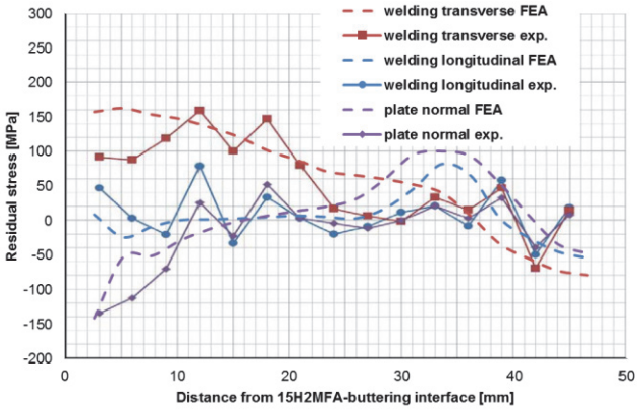

Figure 13: Estimate of residual stresses along a line 33.33 mm from the specimen surface.

Near the centre of the plate (Fig. 12) tri-axial compression was found. In this case the highest compression of about -400 MPa is found in the welding transverse and through thickness directions, whereas the welding longitudinal component exhibits -200 MPa only. 6.66 mm from the lower surface of the mock-up almost no residual stresses have been obtained for the welding direction (Fig. 13), and a small amount of tensile stress for the welding transverse direction and an even smaller amount of compressive stress in the through thickness direction [2].
The simulations predict a range in residual stress components achieving good agreement near the outer surfaces, but the ferritic section of the mid-thickness comparison show that there are some deviations between the predictions and the measurement.
In Fig. 12, although calculated the longitudinal residual stress distribution shape is similar to the measured by the experiment near the weld zone, the magnitudes predicted by the numerical model are significantly lower than the measured data.
One possible reason is the calculated yield strength of the base metal for each phases used in the FE model. It seems to be the yield strength variation during the cladding and welding passes resulting in the difference between the predictions and the measurements.

One should also note that any effects of phase variations are not yet seen by the neutron measurements, as no reference specimen could be measured so far. One remarkable observation from these results is that in no case the welding longitudinal direction exhibits the highest residual stresses, neither in tension nor in compression [2].

SUMMARY

In this study, residual stress prediction was carried out for dissimilar metal welded mock-up. Three-dimensional model was utilized to predict stress fields after welding, especially the longitudinal residual stresses which are in general most harmful to the integrity of the structure among the stress components, in dissimilar steel butt-welded joints between ferritic and austenitic steels which are in essence have different thermal and mechanical properties.
All results are presented considering temperature dependent material properties, phase change, and convection boundary. Also, experimental measurements employing neutron diffraction have been conducted to assess residual stresses within the welded samples. An acceptable agreement has been found between the predicted and the measured data that verifies the validity of the employed model. The simulation results suggest obtaining a highly precise prediction of final residual stress in the joint of the dissimilar metals. Furthermore, considering the important manufacturing processes and developing more reasonable material models are necessary. Both the numerical model and the experiment show that strain hardening consent to the final residual stresses.

ACKNOWLEDGEMENT

The presented work was carried out as a part of the MULTIMETAL project that has received funding from the European Community's Seventh Framework Program (FP7/2012- 2015) under grant agreement n°295968.

REFERENCES

[1] Szavai, Sz., MULTIMETAL Deliverable D3.3 VVER type mock-up. Manufacturing report, BZF, (2012).
[2] Ohms, C., Martin, O., Bezi, Z., Beleznai, R., Szavai, Sz., MULTIMETAL Deliverable D3.10, Residual Stress Measurements of Mockup-3. Technical report, JRC, BZF, (2015).
[3] Goldak, J., Chakravarti, A., Bibby, M., A new finite element model for welding heat sources model. Metallurgical Transactions B., 15B (1984) 299-305.
[4] Lindgren, L.-E., Runnemalm, H., Näsström, M., Simulation of multipass welding of a thick plate. International Journal for Numerical Methods in Engineering, 44(9) (1999) 1301-1316.
[5] MSC.Marc 2013.1 Volume A: Theory and User Information.
[6] Smith, M.C., Smith, A.C., Wimpory, R., A review of the NeT Task Group 1 residual stress measurement and analysis round robin on a single weld bead-on-plate specimen, International Journal of Pressure Vessels and Piping, (2014) 93–140.
[7] Saunders, N., Guo, Z., Li, X., Miodownik, A.P., Schillé, J.P., The calculation of TTT and CCT diagrams for general steels, Internal report, Sente Software Ltd., U.K., (2004).